Atmospheric Research 277 (2022) 106316

Contents lists available at ScienceDirect

Atmospheric Research

journal homepage: www.elsevier.com/locate/atmosres

Meteorological factors in the production of gigantic jets by tropical thunderstorms in Colombia

Oscar A. van der Velde *, Joan Montanyà, Jesús A. López

Department of Electrical Engineering (DEE), Lightning Research Group, Universitat Politècnica de Catalunya BarcelonaTech (UPC), TR1, Colom 1, 08222 Terrassa, Spain

ARTICLE INFO

Keywords:
Thunderstorms
Gigantic jets
Climatology
Statistics
ERA5
Tropical convection

ABSTRACT

Gigantic jets are electric discharges that on rare occasions can be seen at night shooting out of the top of tropical thunderclouds, reaching the ionosphere (90 km). Using sensitive camera systems and detection software, we recorded 70 events over northern Colombia and adjacent seas, most of them captured between 2016 and 2022. This is the first study to compare the meteorological background conditions for thunderstorms that produced gigantic jets in 48 nights against 83 reference cases with monitored thunderstorms that did not produce jets, using vertical profiles from ERA5 reanalysis near the event location. From the vertical profiles, various meteorological parameters are calculated, grouped by metrics of the low level convective parcel, instability, humidity, warm cloud and mixed phase parameters, and vertical wind shear, not limited to default levels.

We report statistically significant differences and effect sizes (Cohen's d) for gigantic jet producing environments compared to null environments. Gigantic jets are produced in conditions with reduced low level temperatures in combination with warmer mid levels. This causes a lower cloud base and higher −10 °C isotherm altitude, thus a greater warm cloud depth, as well as reduced updraft and downdraft buoyancy. Over northern Colombia the non-GJ producing storms tend to grow in an environment that supports more vigorous, multicellular convection by enhanced low-level storm-relative winds and stronger downdrafts. Over western Colombia, the non-GJ cases tend to have a lower equilibrium level while having favorable warm cloud parameters. No evidence is found for hypotheses that upper level vertical wind shear enables gigantic jet production, nor are overshooting tops larger. The findings can be used for forecasting gigantic jets and their climatologically optimal regions on Earth.

We speculate that the environmental conditions shift the droplet size distribution towards larger drops at the cost of cloud droplets, with enhanced droplet shattering ice multiplication processes as they freeze. Depending on convective evolution, low rime accretion rates could briefly expand the negative charge region downward by inverse polarity charging while the upper positive charge concentration may weaken at the same time, which could lead to a temporary negatively imbalanced electric potential distribution in the cloud needed for gigantic jet emission.

1. Introduction

A gigantic jet (GJ) is an electrical discharge which escapes the top of thunderclouds, traverses the stratosphere and mesosphere, connecting directly to the base of the ionosphere at 60–90 km altitude. Discovered in 2002 (Pasko et al., 2002; Su et al., 2003), gigantic jets were a late addition to the family of transient luminous events (TLE) visible (or detectable) in the night sky above thunderstorms triggered by electrostatic and electromagnetic mechanisms. In contrast to sprites and elves, which can be observed by the hundreds per year by observers in the mid-latitudes (Arnone et al., 2020; van der Velde and Montanyà, 2016), gigantic jets are far less often observed, and almost exclusively over tropical thunderstorms (Chen et al., 2008; Chern et al., 2014; Lazarus et al., 2015). The question of why these events seem confined to tropical conditions, and (even there) are produced very infrequently by thunderstorms, is the inspiration for this work.

A mechanism for jets to escape the thundercloud was proposed by Krehbiel et al. (2008). Analogous to cloud-to-ground lightning, which escapes the bottom or side of the cloud, an imbalance between opposite polarity cloud charge regions can direct the discharge through the

* Corresponding author.
E-mail address: oscar.van.der.velde@upc.edu (O.A. van der Velde).

https://doi.org/10.1016/j.atmosres.2022.106316
Received 2 June 2021; Received in revised form 18 June 2022; Accepted 19 June 2022
Available online 24 June 2022

weaker charge region out of the cloud. The typical polarity of tropical gigantic jets is negative (e.g. Pasko et al., 2002; Su et al., 2003; Soula et al., 2011; Cummer et al., 2009; Lu et al., 2011; Liu et al., 2015; van der Velde et al., 2019), referring to the charge that flows upward. In case of negative gigantic jets, the discharge would develop between a relatively strong mid level negative charge center and a weakened upper positive polarity charge region, which normally should be comparable in magnitude, as explained by Krehbiel et al. (2008). They suggested that mixing of the negative screening layer at the top surface of the cloud with the upper positive charge region could neutralize a fraction of the positive charge to create an imbalance needed for the discharge to acquire a large negative potential and escape.

Several factors have been suggested that could help create an imbalanced charge structure. Turbulence is the mechanism responsible for mixing. As thundercloud tops are turbulent by the nature of convection, extra turbulence in the normally stable environment near the cloud top may be created by greater buoyancy and stronger vertical wind shear. A summary of the shear environment in previous cases and measurements of turbulence in a Florida multiple GJ-producing storm has been provided by Lazarus et al. (2015). Strong wind shear may also cause a differential advection of the upper positive charge region with respect to the central negative charge region, as was proposed by van der Velde et al. (2010). In that case, an unusual positive polarity GJ was produced by a low-topped Mediterranean winter thunderstorm, with winds over 30 m s^{-1} reported at the cloud top with weaker winds below. In the same geographic region, van der Velde et al. (2013) reported strong vertical shear and dry air in cases of cloud-to-air lightning discharges reaching 1–3 km out of the cloud top. Lazarus et al. (2021) reported on the effect of gravity wave breaking at the cloud top to mix and dilute the screening layer and upper positive charge region. They also reported a very narrow layer with strong vertical wind shear at the cloud top.

Another hypothesis, proposed by Soula et al. (2011), is the dispersion of the upper positive charge relative to the central negative charge region, due to a rapidly expanding anvil cloud. Additionally, Boggs et al. (2018) simulated the electrical effect of an overshooting top with a narrowed upper positive charge region geometry, which appeared beneficial for guiding the discharge upwards out of the cloud. These two mechanisms do not require enhanced vertical wind shear.

Another hypothesis is the build-up of a large quantity of negative charge by reduction or elimination of competing intracloud and (especially) cloud-to-ground lightning discharges. There has been some support for this in the cases of van der Velde et al. (2007, 2010), Soula et al. (2011) and Meyer et al. (2013), where low cloud-to-ground flash rates were observed in the minutes prior to gigantic jet production. For this to happen, an absent or instead a too strong lower positive charge region could cause lightning to either not initiate in the lower half of the cloud, or to initiate only low-altitude intracloud flashes. The relative vertical spacing and altitude of charge regions (see López et al., 2019 for Colombian storms) may also control the initiation rates.

This work uses our database of events recorded by cameras operated in Colombia that monitor the occurrence of transient luminous events over several of the most intense nocturnal lightning and precipitation hotspots in South America (Albrecht et al., 2016; Mapes et al., 2003). For the scope of this paper, we investigate factors in the meteorological environment of thunderstorms that may enable the occurrence of gigantic jets. We examine the vertical distribution of wind, temperature and humidity from reanalysis data for 49 different gigantic jet cases recorded in and around Colombia and compare these parameters to a null dataset of 83 cases where sprites or distant lightning flashes were observed in the same region under clear night sky without any detected gigantic jets.

2. Methods

2.1. Observation

Gigantic jets were observed using a low-light video detection system based on a Watec camera with 1/2″ charge-coupled device (CCD) sensor mounted with a 8 mm F1.2 lens providing a horizontal angle of view of about 43°. Event detection was handled by SonotaCo UFOCapture software. The time was synchronized by Global Positioning System (GPS) or Network Time Protocol (NTP) to a precision of <1 s. The camera, mounted on a pan-tilt unit, was first installed on the island of San Andrés of Colombia (2009–2014) in the southwestern Caribbean Sea, and was moved in 2016 to the campus of Universidad del Magdalena in Santa Marta at the north coast of Colombia. Another camera (without pan-tilt) was added in Manizales in summer 2019, observing the sky over the west coast. An example gigantic jet image from that camera is shown in Fig. 1. A similar system was operational at the weather service of Curaçao between 2014 and 2018, aiming to northwestern Venezuela, but did not observe gigantic jets, and was subsequently located in Barranquilla city in Colombia from 2019 to 2021. Additional gigantic jets have been observed during campaigns in 2017 and 2018 (van der Velde et al., 2019).

Table S1 in the supporting information lists the 70 gigantic jets observed in 48 nights (1 night had one gigantic jet case in northern Colombia and one case in western Colombia, which count as separate cases). For the purposes of this study the events are separated into three regions: Caribbean Sea (24 GJ events in 17 nights), northern Colombia (24 GJ events in 20 nights), and western Colombia (22 GJ events, 12 nights).

2.2. Reanalysis data

In this study we use the Copernicus Climate Change Service ERA5 reanalysis data set at pressure levels (Hersbach et al., 2020), which assimilates meteorological data and interpolates it to grid cells of 30 km. Output is available at 1-h intervals with a horizontal latitude-longitude grid spacing of 0.25° and vertical intervals of 25 hPa between 100 and 300 hPa and between 1000 and 700 hPa, with 50 hPa intervals between 700 and 300 hPa. Parent thunderstorms were found using time, azimuth and elevation of the gigantic jets, combined with GOES satellite data and *Keraunos* lightning detection network data (Aranguren et al., 2014). A single vertical profile was taken within 0.5° latitude/longitude from the

Fig. 1. Example of a gigantic jet captured by the camera installed in Manizales. This event occurred on 23 August 2021 at a distance of 113 km over the lowlands of Choco, western Colombia. The thunderstorm top is visible at the very bottom.

jet location, by considering the situation in the ERA5 fields using the roaming sounding and hodograph functionality in McIDAS software. None of the profiles were taken above mountainous terrain. The average deviations are 0.1° north and 0.03° west of the GJ location. Based on the 1000 hPa level equivalent potential temperature field and low-level convergence pattern, the profile was picked where Convective Inhibition (CIN) was closest to zero. Usually (in 76% of GJ cases) these conditions were found in the ERA5 within 0–2 h before the storm that produced the jet (on average 1 h). In 8 cases (16%) the ERA5 produced detectable convective development earlier than observed and we picked the profile 3 or 4 h earlier when the convergence zone and CIN minimum were close to the GJ location prior to the convection-induced cooling near the surface in the ERA5. In another 8% of cases the profile time was up to 2 h after the real time of occurrence.

For the calculation of parcel theory parameters we use the mixed-layer parcel, obtained as the averaged absolute humidity and potential temperature (θ) values over the lowest 50 hPa (~500 m, levels 1000, 975 and 950 hPa). Although it is night, we found little use for the "most unstable" parcel method as there are no elevated warm layers or ground inversions in the extracted profiles in this study.

As McIDAS software did not save a correct altitude for each pressure level, the (geopotential) altitudes are computed by integrating the hypsometric equation above the 1000 hPa level using the virtual temperature profile, added to the ERA5 1000 hPa (geopotential) altitude.

In the discussion of the results we will refer to the "low levels" as 1000–700 hPa (0–3 km), "mid levels" as 700–300 hPa (3–9 km), "upper levels" as 300–150 hPa (9–13.5 km), and "top levels" as 150–100 hPa (~13.5–16.5 km).

2.3. Null cases

The ideal null case is one where we can be certain that no gigantic jet was produced by any storm in the region monitored. This excludes many thunderstorm nights where clouds prevented the clear sky above to be monitored. The best set of null cases, over northern Colombia, has been selected from Santa Marta data in which no GJ events were detected, where the sky was mostly clear, the camera pointed at active storms for a long period of time and detected distant lightning flashes or sprites to be sure of proper operation and detectability. Only one representative profile was selected per night.

The second best set comprises similar nights over western Colombia, observed from Manizales city. However, at that location it is almost impossible to avoid some short periods with clouds, and thunderstorm activity tends to be well developed including before nightfall and after daybreak. This makes it more likely that a GJ may have been missed, even though the camera observed many hours of active storms without events. Because of the long-lasting activity during these nights and the different locations of storms (across the same region as the GJ events) it was decided to select two profiles per night at optimal locations, thought to be most representative of the evening and early morning hours activity. For the statistical significance and effect size calculations we used the number of null cases instead of the number of profiles. Null cases and GJ events are counted as separate cases with unique profiles when occurring in different regions (Caribbean lowlands versus Pacific lowlands), even if they occurred during the same night.

Although our selection process for null cases attempts to minimize the chances an event could be missed, it can never be ruled out that a gigantic jet did occur after all, e.g. produced by a storm outside the camera's view, by a more distant storm than the one observed, during brief periods of visually undetectable cloud, a short-lasting software malfunction or dead time, or the daylight period.

The profile selection has been performed in the same way as for GJ cases. We believe any bias involved in manually selecting profile locations to be minimal. The visual clues of wind shear, humidity and instability in the GJ and null case soundings often appeared mutually interchangeable, and in fact the outcome of the statistics was different from expectations. In Sections 3.9 and 3.10 we investigate the robustness using an alternative method.

2.4. Methodology

The aim of this study is to describe the central tendencies in the meteorological profiles per group and highlight any important differences between gigantic jet-producing and null case environments and their geographical regions. The table of all GJ events is provided as supplementary data. It is important for the proper interpretation of the results to eliminate possible meteorological differences created by topographic effects. For example, the low-level winds generally blow from the east-northeast across the Caribbean (trade winds), but shift to northwesterly directions over northern Colombia. The Caribbean also tends to have drier air in the middle troposphere (Dunion, 2011). We therefore divided cases into three geographical categories, northern Colombia (Caribbean lowlands), western Colombia (Pacific lowlands) and the southwestern Caribbean Sea. The latter contains cases observed from San Andrés together with maritime cases observed from Santa Marta closer to the Colombia and Panama coast.

We summarize in tables the central tendency and results of the statistical significance test for various parameters. All parameter values are assumed to be samples from a normal distribution, but with different variances for GJ and null populations, for that reason the Welch unequal-variances two-tailed *t*-test was selected for statistical significance calculation (Ruxton, 2006; Delacre et al., 2017). We consider the 99% significance level ($p < 0.01$) in order to reject the null hypothesis that the GJ and null distributions are identical, but will discuss marginal significance (95%, $p < 0.05$) as well. We express the effect size by Cohen's *d*, which is the difference between the means normalized by the pooled standard deviation (e.g. Lakens, 2013 and references therein). Here, values >0.6 are deemed meaningful.

3. Results

3.1. Geographical and temporal distribution

Fig. 2 shows a map of all GJ locations (a), their ERA5 profile locations over northern Colombia (b) and the locations of the profiles for the null cases in the same region (c). It can be noted how many of the GJs over Colombia occur over the lowlands, but close to the transition to elevated terrain (contoured). Typically no storm motion could be observed between the time of storm inception and the occurrence of a GJ. The null cases concentrate a bit further north within the Caribbean lowlands. This is because of the criterion that electrical activity (lightning or sprites) must be clearly observed by the camera in Santa Marta, to minimize the chance of missing a gigantic jet, even though gigantic jets and sprites have been detected much farther away. The color of the location markers indicates that gigantic jets tend to occur later during the night (see also Fig. S1). The null cases indicate that there is certainly no lack of thunderstorm activity earlier in the night. Most GJ events recorded from Santa Marta occurred between the start of June and early December, peaking slightly between mid-October and early December. The null cases reflect the same distribution. In Manizales the observation period was too short to be able to point out a time of the year that stands out as the most productive.

3.2. Vertical profiles of temperature and humidity

Fig. 3 presents the mean temperature and dewpoint profiles of GJ associated storms in northern Colombia (red), the Caribbean (teal), western Colombia (magenta) and null cases over northern (blue) and western Colombia (black), in the form of the equivalent potential temperature plot (also known as *Theta-plot*, Morgan, 1992; Manzato and Morgan, 2003). This is a thermodynamic diagram where moist adiabatic processes in convective updrafts occur along vertical lines of constant

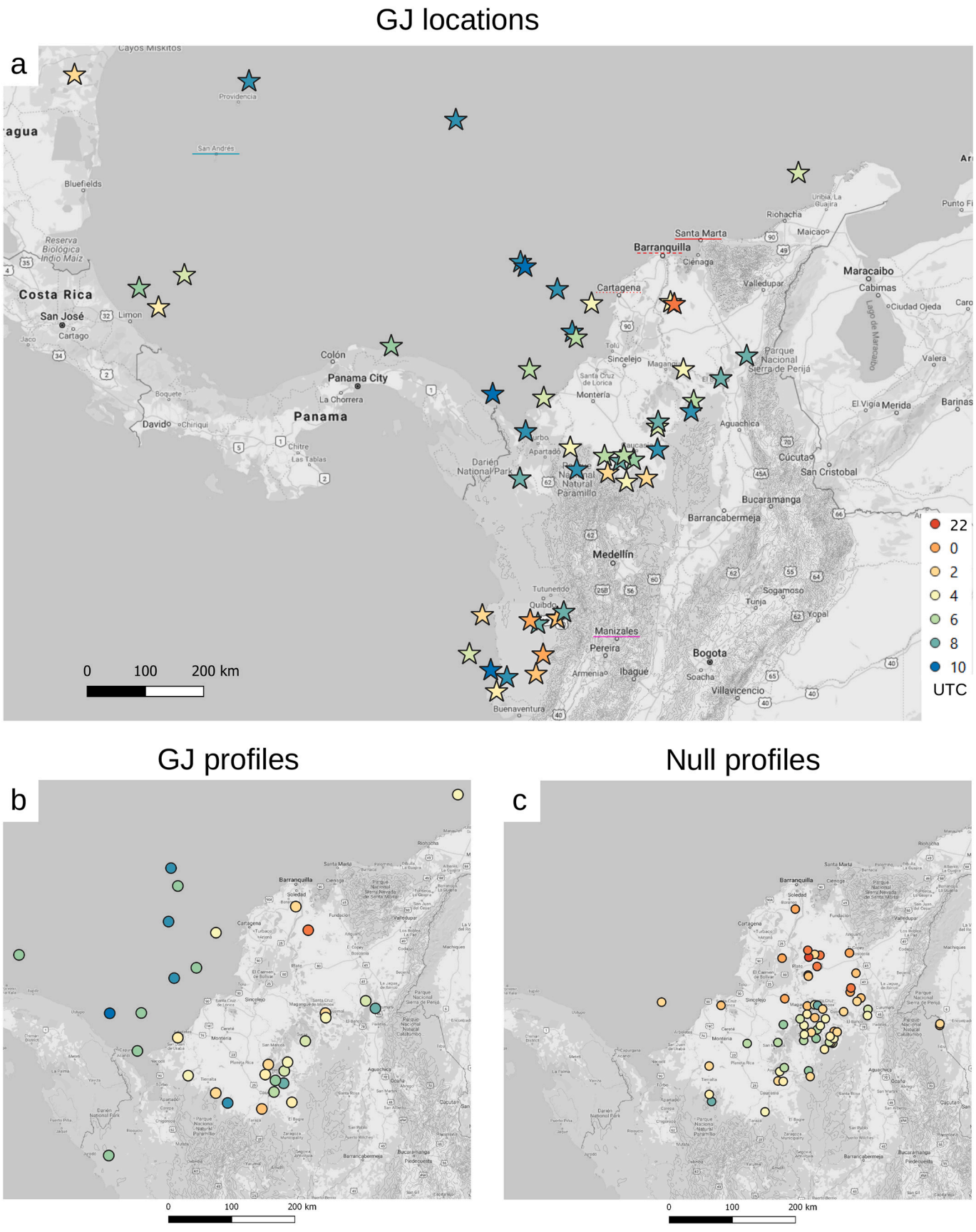

Fig. 2. (a) Map of gigantic jet locations over western and northern Colombia and adjacent Caribbean Sea. The marker color represents the time of occurrence. The locations of the six northwestern-most Caribbean cases are less precise. (b) Zoomed in map of locations of the ERA5 profiles selected for gigantic jet cases, and their times. (c) Zoomed in map of of locations of the ERA5 profiles selected for null cases, and their times.

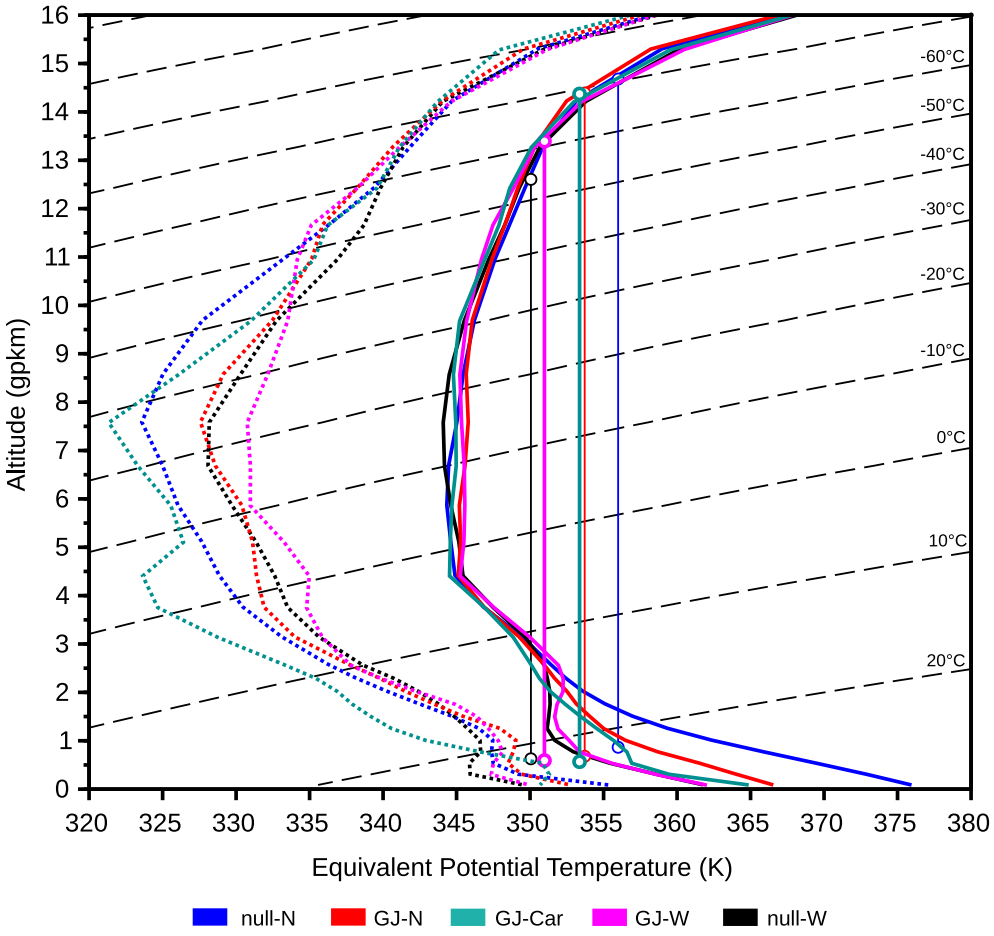

Fig. 3. Thermodynamic diagram in the Theta-plot style for mean conditions associated with null and gigantic jet cases over northern and western Colombia and the Caribbean, as indicated by the legend, with mean temperature (solid lines), dewpoint (dashed lines), saturated parcel trajectories (fine vertical lines), the lifting condensation level or approximate cloud base (bottom circles) and equilibrium levels (top circles). Isotherms are plotted as diagonal dashed lines.

equivalent potential temperature θ_E, which is a conserved property. The temperature and dewpoint profiles (right and left respectively) have been translated into θ_{ES} by assuming the saturation mixing ratio corresponding to their temperature and pressure (hence the subscript $_S$). During saturated ascent θ_E is equivalent to θ_{ES} of the parcel. All equivalent potential temperature values have been calculated using the formula by Bolton (1980).

The ambient vertical temperature gradient becomes weaker around 14 km altitude, before becoming absolutely stable above the tropopause, generally above 16 km in this region (not shown). Exact tropopause heights could not be determined, as relatively coarse resolution pressure-level ERA5 data is used here instead of the native model-level ERA5 data.

Mean profiles show only subtle differences between the three GJ and two null categories in mid and upper levels. The mean null profiles are slightly cooler in the mid levels. In the low levels the mean GJ profiles are clearly cooler than the mean null profile of northern Colombia, but warmer than the mean null profile of western Colombia. It appears that the mid levels are more humid in the GJ profiles and western Colombia null profiles, while the Caribbean sea and northern Colombia null profiles are drier. The nearly moist-adiabatic layer at 1–2 km altitude in western Colombia may be a result of westerly low level upslope winds, or from advection of cooler Pacific air in the low levels below easterly flow (above 2 km). In addition, there are distinct visual differences between the vertical lines representing the parcel (updraft) temperature. These details are discussed in the next sections.

3.3. Near-surface parameters

We start our parameter discussion near ground level. The properties of absolute moisture content and temperature in the boundary layer are basic ingredients that determine the convective cloud base height, cloud top and the buoyancy in the cloud, discussed in Section 3.4. Table 1 summarizes the statistical differences between the three categories. The differences in mixed-layer absolute humidity (mixing ratio of water vapor to dry air, r) are very small: a mean of ~18.0 g kg^{-1} is found in northern Colombia and Caribbean GJ and null cases. The western Colombia GJ and null groups show slightly lower mixing ratios than in the other regions. The mean potential temperature θ is 1.6 K lower for the GJ cases compared to null cases in northern Colombia, with large effect size (1.09). The western Colombia and the Caribbean GJ and null cases are 0.7 to 1 K cooler than in northern Colombia. Theta-E (θ_E) is constant along the parcel trajectory. It represents both the parcel temperature and moisture in the saturated phase. The mean mixed-layer θ_E for the null category is 2.3 K higher than for the GJ over northern Colombia. Of the three regions, western Colombia has the lowest values for these three parameters. As will be shown in the next section, this is reflected also in the instability parameters.

3.4. Instability parameters

Parcel theory (e.g. Wallace and Hobbs, 2006) describes the temperature evolution a parcel of air will experience when lifted adiabatically. In Fig. 3, we plotted the saturated portion of the mixed layer parcel

Table 1
Mean mixed layer values, statistical significance and effect size for near-surface parameters for the GJ cases and null cases by region. Values in bold indicate significant differences (Welch *t*-test $p < 0.01$ and Cohen's d > 0.6) between GJ and null categories.

Parameter	N Colombia		W Colombia		Carib. Sea	p-value			Cohen's d		
	Null (61)	GJ (20)	Null (22)	GJ (12)	GJ (17)	NCol	WCol	All	NCol	WCol	All
r (g kg^{-1})	18.10	17.97	17.20	17.49	18.15	0.55	0.07	0.25	0.12	0.67	0.19
θ (K)	**302.3**	**300.7**	299.6	299.6	300.0	**7e-7**	0.92	**1e-4**	**1.09**	0.03	**0.60**
θ_E (K)	**356.0**	**353.7**	350.1	351.0	353.4	**4e-3**	0.33	0.21	**0.66**	0.36	0.20

ascent trajectories. Conditional instability is present when the parcel θ_E is warmer than the θ_{ES} environment. In that figure, the bottom circles indicate the Lifting Condensation Level (LCL, approximating the cloud base), the top circles the Equilibrium Level (EL, the average convective cloud top without overshoot). We used the virtual temperature correction in the calculation of Convective Available Potential Energy (CAPE) and Convective Inhibition (CIN), which accounts for the reduced volumetric density of dry air with water vapor mixed in. Because of the dependency of CAPE on the θ_E of the parcel (correlation coefficient $R = 0.96$) and the temperature profile of the environment, similar tendencies are found (Table 2): the GJ cases over northern Colombia have a mean CAPE about 26% lower than the null cases in that region (Cohen's d 0.75). The CAPE values for gigantic jets never reached over 2203 J kg^{-1} in this data set. However, 43% of the null cases exceeded that, up to a maximum of 3765 J kg^{-1}. A boxplot for CAPE is included in Fig. 4. The Caribbean GJ cases have similar CAPE mean values as well as a similar maximum of 2271 J kg^{-1}. For western Colombia the low-level moist adiabatic layer seen in Fig. 3 is responsible for the generally weaker instability. The mean CAPE is considerably lower than in the other regions (975 J kg^{-1} compared to 1500–1700 J kg^{-1}), including for the null cases, while the maxima peak at 2117 and 2583 J kg^{-1} respectively.

The Lifted Index (LI) represents the buoyancy at the 500 hPa level. The version based on the most unstable parcel (highest θ_e) in the low levels performs better than other buoyancy parameters, with a Cohen's d of 1.22 in northern Colombia and 0.67 overall.

Mean CIN values (−9 to −22 J kg^{-1}) are not large and do not differ significantly between groups. This is an expected result of the profile selection methodology looking for minimized CIN. Related to this, the Level of Free Convection (LFC) is not statistically different between groups either.

For the EL we find insignificant differences at the 99% level, with a (mixed layer) parcel stabilizing on average above 14.3 km (Fig. 4b). The GJ-related EL heights range between 12.2 and 15.6 km geopotential altitude. It is interesting to note that in western Colombia, where many parameters show insignificant differences between null and GJ cases, the EL has a relatively elevated Cohen's d of 0.75 but at the current small sample size it is only statistically significant at the 95% level.

The actual maximum cloud top is the altitude where the parcel reaches zero vertical speed after losing kinetic energy to negative buoyancy beyond the EL. This maximum parcel level (MPL) represents the overshooting top height. Table 2 shows no difference between null and GJ cases for this parameter. However, when considering the difference MPL-EL, the overshooting top size, there is a slight (Cohen's d 0.59) and statistically significant difference between GJ and null overall, with the GJ events having on average 200–300 m smaller overshoot. Although this is statistically not a very strong signal, it is better than for other updraft buoyancy related parameters. The minimum MPL height for GJ is 15.4 km. The maximum MPL height found in this dataset is 19.8 km.

We calculated the negative downdraft buoyancy DD $\Delta\theta_{ES}$ measured at the 950 hPa level, using the ambient 500 hPa θ_E for the saturated downdraft parcel trajectory. Positive values here mean the downdraft is colder than the low level ambient air. This parameter shows an enhanced effect size (1.29) and significance levels for northern Colombia, but not in the other areas where low values are seen also in null cases (Fig. 4c). The 500 hPa θ_E contributes to a 2° warmer downdraft in GJ cases in the northern area, but most of the reduced downdraft buoyancy in GJ profiles is due to the weaker lapse rates.

3.5. Humidity parameters

The Lifting Condensation Level (LCL) is the approximate cloud base height and is a parcel parameter that is directly related to the dewpoint depression and relative humidity near the surface (mixed lowest 500 m layer). As seen before, the most pronounced differences are observed over northern Colombia, with the null cases showing a mean LCL of 867 m and the GJ a mean of 679 m above sea level (Table 3). Over the Caribbean Sea and in western Colombia, the cloud base is lower (567 and 593 m). The temperature at the cloud base (TLCL) is marginally higher for GJ compared to null groups.

In Fig. 3, a difference can be noted in the dewpoint curves (dashed lines), suggesting the null cases over northern and western Colombia have drier profiles than the GJ. However, differences in relative humidity (RH) in the mid (600 hPa) and upper (300 hPa) levels are not statistically significant. A highly significant difference is found for 925 hPa RH (Fig. 4d), near the cloud base level. Here all GJ categories have a mean humidity of 87–93%, whereas the null over northern Colombia is less humid at 79% (Cohen's d 1.06). The null cases of western Colombia, however, are just as humid as the GJ cases in that area.

Precipitable Water (PW, boxplot in Fig. 4e) is the water vapor content integrated over a vertical column. The differences between groups are not significant at the 99% level. The values for GJ are lower than

Table 2
Mean values, statistical significance and effect size for parcel and instability parameters for the GJ cases and null cases by region.

Parameter	N Colombia		W Colombia		Carib. Sea	p-value			Cohen's d		
	Null (61)	GJ (20)	Null (22)	GJ (12)	GJ (17)	NCol	WCol	All	NCol	WCol	All
CAPE (J kg^{-1})	**2084**	**1549**	852	975	1636	**1e-3**	0.43	0.16	**0.76**	0.28	0.22
LI (K)	**−4.8**	**−3.6**	−2.5	−2.4	−3.7	**1e-4**	0.90	0.02	**1.05**	0.04	0.39
LI_{MU} (K)	**−6.3**	**−4.5**	−3.5	−3.3	−4.1	**3e-6**	0.61	**7e-5**	**1.22**	0.17	**0.65**
CIN (J kg^{-1})	−23	−19	−19	−18	−9	0.13	0.86	**9e-3**	0.35	0.06	0.43
LFC (hPa)	859	861	839	831	889	0.82	0.75	0.18	0.06	0.11	0.23
EL (km)	14.67	14.38	12.60	13.39	14.36	0.20	0.04	0.21	0.34	0.72	0.21
MPL (km)	18.18	17.70	16.27	16.71	17.70	0.02	0.21	0.96	0.63	0.43	0.01
MPL-EL (km)	3.51	3.32	3.67	3.32	3.34	0.01	0.05	**8e-4**	0.61	0.65	**0.59**
DD $\Delta\theta_{ES\ 950}$ (K)	**32.9**	**23.0**	17.4	16.7	20.4	**8e-10**	0.77	**1e-5**	**1.29**	0.10	**0.69**
(DD) $\theta_{E\ 500}$ (K)	**336.5**	**338.6**	338.0	338.0	336.5	**6e-3**	0.28	0.10	**0.69**	0.38	0.29

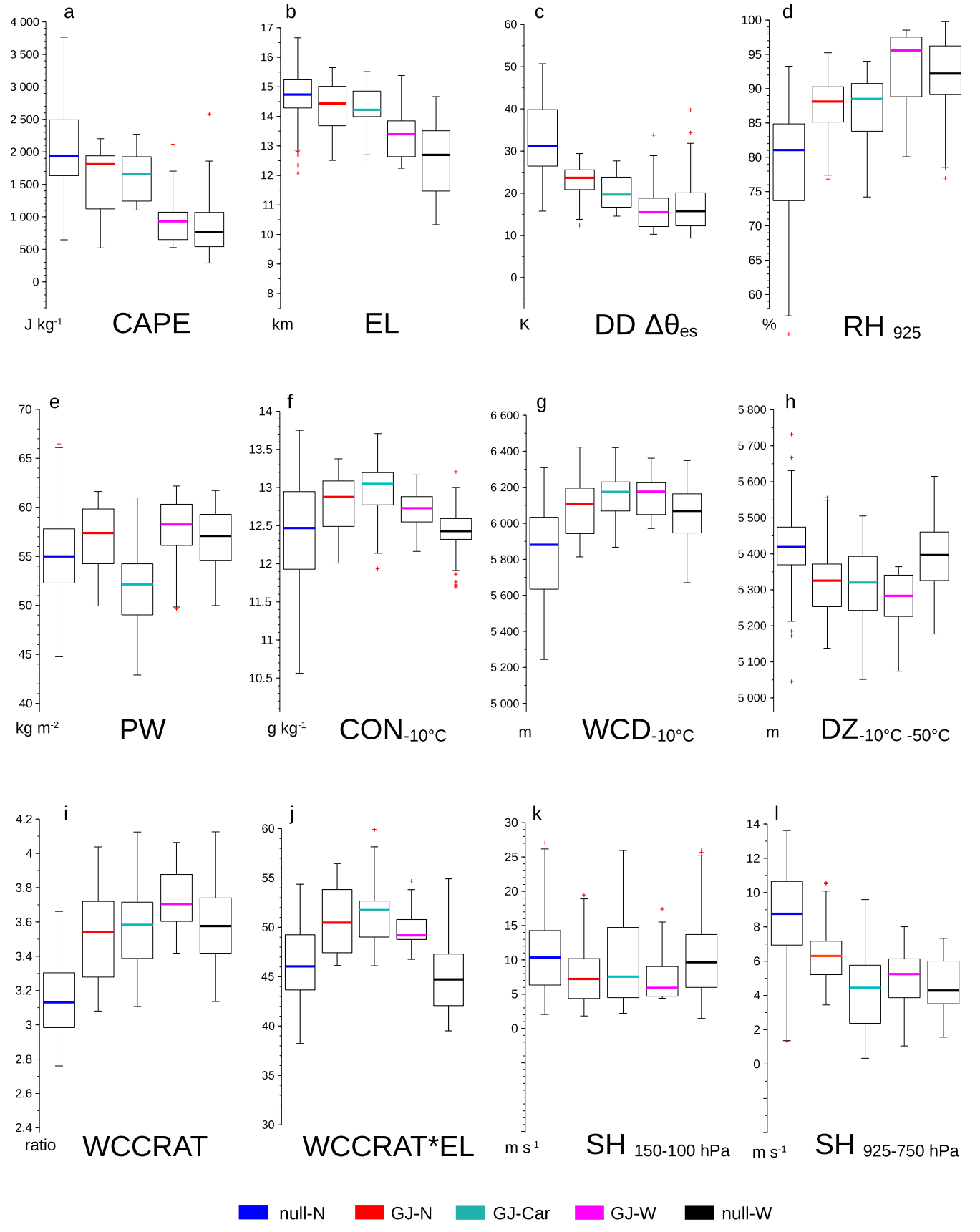

Fig. 4. (a-l) Selected boxplots for the distribution of various parameters for null and gigantic jet cases over northern Colombia (blue and red), gigantic jet cases over the Caribbean Sea (teal), and gigantic jet and null cases over western Colombia (magenta and black).

Table 3
Mean values, statistical significance and effect size for humidity parameters for the GJ cases and null cases by region.

Parameter	N Colombia		W Colombia		Carib. Sea	p-value			Cohen's d		
	Null (61)	GJ (20)	Null (22)	GJ (12)	GJ (17)	NCol	WCol	All	NCol	WCol	All
LCL (m)	**867**	**679**	628	593	567	**5e-6**	0.50	**2e-6**	**0.84**	0.23	**0.75**
TLCL (K)	294.7	295.0	294.4	294.7	295.3	0.25	0.04	**3e-3**	0.21	0.70	0.47
RH_{300} (%)	36.6	48.5	49.2	50.6	45.7	0.02	0.79	0.04	0.64	0.09	0.37
RH_{600} (%)	65.5	70.0	72.3	77.1	56.4	0.14	0.16	0.69	0.45	0.35	0.08
RH_{925} (%)	**78.8**	**87.5**	91.6	93.0	87.0	**5e-7**	0.53	5e-4	**1.06**	0.22	0.56
PW (kg m^{-2})	55.0	57.0	56.6	57.9	51.9	0.04	0.28	0.83	0.50	0.41	0.04
SD (kg m^{-2})	**20.9**	**16.3**	14.3	13.8	19.9	**7e-6**	0.75	0.13	**1.02**	0.11	0.26

previously reported cases (e.g. Soula et al., 2011) where it was around 65 kg m^{-2} which is nearly the maximum of our data set. The Caribbean profiles featured somewhat lower PW in agreement with the lower dewpoint temperatures between 1 and 9 km altitude in Fig. 3. Similar to PW, the saturation deficit can also be integrated over a vertical column (SD). Over northern Colombia this parameter confirms GJ conditions clearly closer to saturation than the null cases (Cohen's d 1.02). Over western Colombia, both GJ and null are equally humid. Like PW, the Caribbean SD values also indicate drier conditions.

3.6. Warm cloud and mixed phase parameters

This section discusses parameters related to temperature levels loosely associated with important microphysical and electric charging processes. First, we start with several temperature levels (Table 4): 0 °C, −10 °C, −30 °C and − 50 °C. Here we do not see differences at the 99% confidence level. However, the −10 °C level does show a significant but modest difference (Cohen's d 0.53) in the total GJ-null comparison. The Caribbean GJ set has systematically slightly cooler profiles (lower heights) than the other regions. The altitudes of −10 °C to −30 °C correspond well with the main negative charge region in Colombian thunderstorms in López et al. (2019), while the −50 °C altitude corresponds to the lower limit of the upper positive charge region during the peak lightning activity of the storms in that study.

Warm cloud depth (WCD) indicates the depth over which condensed water exists between the LCL and the freezing level. A larger WCD benefits coalescence processes between growing rain droplets, which promotes rain falling out of the updraft before it freezes. The WCD clearly exhibits tropical values here (full range: 3415–4770 m), due to the high freezing level and low LCL. The lowest mean value corresponds to the northern Colombia null case group. However, the difference is mainly due to the LCL contribution. WCD calculated using the −10 °C level performs better (Cohen's d of 1.08 for northern Colombia, 0.99 for the GJ and null of all regions combined, boxplot shown in Fig. 4g). We found a significant GJ-null discrimination both in northern and western Colombia for the vertical distance between the −10 °C and − 50 °C levels (Cohen's d 0.93 and 1.33 respectively, listed as $DZ_{-10\ -50°C}$ in Table 4, boxplot Fig. 4h). It is smaller for the GJ cases, due to warmer mid levels (higher −10 °C altitude) and slightly colder upper levels (lower −50 °C altitude). When combined with warm cloud depth as the ratio we define as WCDRAT = $WCD_{-10°C}$ / $DZ_{-10\ -50°C}$, it performs better still (Cohen's d 1.38, 1.28, 1.28 respectively for northern, western, and all areas combined).

Similar to the depth of microphysical regimes in the cloud, one may consider the adiabatic condensation produced in warm and mixed phase regimes. A strong signal (Cohen's d of 1.56, 0.64, 0.93) was found for another ratio we defined, the warm/cold cloud condensation ratio WCCRAT. Provided that the parcel trajectory is warmer than the environment, this parameter considers how much water is condensed during parcel ascent between cloud base and the ambient −10 °C level, and between the ambient −10 °C to −30 °C levels: WCCRAT = $(r_{LCL} - r_{sat-10°C}) / (r_{sat-10°C} - r_{sat-30°C})$. Here r_{LCL} is the parcel's original mixing ratio, maintained until reaching the LCL, and r_{sat} is the adiabatic saturation mixing ratio at the temperature and pressure of the parcel. The −10 °C and − 30 °C temperature levels are those that resulted in the best Cohen's d value after experimenting with a range of temperatures at 5 °C intervals. The parameter values range from 2.76 to 4.12, the higher values associated with GJ cases (Fig. 4i). It can be noted that the null cases in western Colombia have a higher mean WCCRAT value than the GJ cases in northern Colombia, which shows the potential difficulties of applying these parameters in forecasting, as will be discussed later. The WCCRAT parameter is correlated with $WCD_{-10°C}$ ($R = 0.78$), WCDRAT ($R = 0.84$) and Lifted Index ($R = 0.82$). Note that the cloud base height is not a factor in this parameter. Interestingly, the numerator of WCCRAT (listed as $CON_{-10°C}$ in Table 4) discriminates well between GJ and null cases in western Colombia (Cohen's d of 0.82, Fig. 4f) where the denominator ($CON_{-10\ -30°C}$), which is strongly correlated with Lifted Index and CAPE, is low.

An interesting relation between WCCRAT and EL height will be discussed in Section 4.1. Here, we list WCCRAT multiplied by EL (in km) (Table 4, last row). Overall, this raises Cohen's d to 1.43, a large improvement compared to those of WCCRAT (0.93) and Z_{EL} (0.72) on their own. In western Colombia, Cohen's d improved to 1.54, but in northern Colombia it decreased (to 1.22) compared to WCCRAT. A

Table 4
Mean values, statistical significance and effect size for warm cloud and mixed phase parameters for the GJ cases and null cases by region.

Parameter	N Colombia		W Colombia		Carib. Sea	p-value			Cohen's d		
	Null (61)	GJ (20)	Null (22)	GJ (12)	GJ (17)	NCol	WCol	All	NCol	WCol	All
$Z_{0°C}$ (m)	4954	4987	4978	4987	4931	0.29	0.85	0.83	0.26	0.07	0.04
$Z_{-10°C}$ (m)	6690	6762	6666	6753	6712	0.02	0.03	**6e-3**	0.61	0.93	**0.53**
$Z_{-30°C}$ (m)	9623	9613	9557	9574	9533	0.81	0.61	0.40	0.07	0.19	0.16
$Z_{-50°C}$ (m)	12,107	12,076	12,068	12,024	12,020	0.30	0.14	0.02	0.27	0.58	0.44
$WCD_{0°C}$ (m)	**4087**	**4308**	4350	4394	4364	**9e-5**	0.45	**4e-5**	**0.86**	0.25	**0.67**
$WCD_{-10°C}$ (m)	**5823**	**6084**	6038	6161	6145	**2e-6**	0.03	**9e-9**	**1.08**	0.79	**0.99**
$DZ_{-10\ -50°C}$ (m)	**5417**	**5313**	**5402**	**5270**	5308	**5e-4**	**6e-4**	**1e-7**	**0.93**	**1.33**	**1.02**
WCDRAT (ratio)	**1.08**	**1.15**	**1.12**	**1.17**	**1.16**	**1e-6**	**1e-3**	**4e-11**	**1.38**	**1.28**	**1.28**
$CON_{-10°C}$ (g kg^{-1})	**12.44**	**12.79**	**12.40**	**12.71**	12.95	**8e-3**	**6e-3**	**9e-6**	0.53	**1.03**	**0.75**
$CON_{-10\ -30°C}$ (g kg^{-1})	**3.96**	**3.65**	3.47	3.41	3.63	**1e-4**	0.41	**1e-3**	**1.04**	0.30	0.57
WCCRAT (ratio)	**3.15**	**3.52**	3.59	3.73	3.58	**8e-6**	0.08	**5e-7**	**1.56**	0.64	**0.93**
WCCRAT*EL	**46.21**	**50.52**	**45.02**	**49.83**	51.33	**2e-5**	**3e-5**	**6e-13**	**1.22**	**1.54**	**1.43**

possible reason for its performance is mentioned in the Discussion (Section 4.2). However, note that the WCCRAT, WCDRAT, $DZ_{-10\ -50°C}$ and WCCRAT*EL parameters introduced here may not necessarily be useful predictors in and outside the tropics without further study.

3.7. Wind profiles and vertical wind shear

It is well known that the variation of wind speed and direction with altitude can significantly impact the character of storms and the distribution of cloud and precipitation particles (e.g. Weisman and Klemp, 1984; Rasmussen and Straka, 1998). In this section we investigate various wind shear parameters.

The shear vector magnitude (SH) between two vertical levels and storm-relative winds (SRW) are directly obtained from the profiles of each case and then compared among groups. We have tested shear vectors for every possible combination of two levels, but highlight only those of interest. The largest significance (Table 5) is found for the shear between the 925 and 750 hPa levels, but only for cases in northern Colombia: a mean of 8.4 m s^{-1} for the null cases, 6.5 m s^{-1} for the GJ cases (Cohen's d of 0.67, Fig. 4l). Investigating this, we found the 750 hPa zonal wind component to be stronger in null cases (median − 5.7 m s^{-1} versus −3.5 m s^{-1} for GJ) with no difference found for 925 hPa wind. The cases in western Colombia and Caribbean Sea show low values of 4–5 m s^{-1}, including the null cases.

The higher layers do not show significant differences at the 99% level, but it can be noted that the upper and top level wind shear means for GJ cases tend to be about 30% lower than for null cases (see Fig. 4k for the cloud top level shear, $SH_{150–100}$). The data do not support the proposed role for increased wind shear at the cloud top in gigantic jet production.

Additionally, the mean density-weighted mean 0–6 km wind has been calculated ($MW_{0–6}$ in Table 5). It is often used to estimate the storm motion. It must be noted that estimated storm motion vectors have not been verified using measurements of the actual storms, and the accuracy for tropical thunderstorms is unknown. Here we subtract the 0–6 km mean wind vector from the wind vectors at each level to obtain storm-relative winds (SRW) for each profile. A moderate low-level storm-relative wind is important for generating new updrafts at outflow boundaries. In the mid and upper levels, stronger storm-relative winds horizontally disperse hydrometeors and may tilt the updraft tower. The vertical profiles (5th, 25th, median, 75th and 95th percentile lines) for northern Colombia are displayed in Fig. 5. For the other regions these profiles are shown in Fig. S2.

Above 350 hPa (8 km) the variability in storm-relative winds within GJ and null categories is large, all the way to the cloud top (14–18 km) and above. The only significant difference in the upper and top level SRW is between GJ and null in western Colombia (between 200 and 100 hPa, Table 5), where the GJ profiles show 26% weaker top level flow. Like for low level shear discussed earlier, a significant difference is found for the mean 1000–700 hPa SRW (Cohen's d 0.81), which applies again only to northern Colombia. Also listed is the mean shear over the 1000–600 hPa layer (MSH). This parameter performs much like low level SH and SRW, but proves more regionally robust in Section 3.9.

3.8. Multiple-GJ cases

The data set contains 14 cases which produced 2, 3 or 4 gigantic jets. We investigated their profile parameters for any differences and similarities. Although there are not many data points per region, they appear to confirm the previous tendencies, in particular for warm cloud and mixed phase parameters. Table 6 presents the comparison of Cohen's d effect sizes for all multi-GJ cases versus all single GJ cases, both in reference to all null cases. WCCRAT*EL shows the best separation for multiple GJ versus null cases overall (1.63). The difference column shows that $Z_{-10°C}$ is particularly enhanced (higher) compared to single GJ cases, as well as the mean 1000–600 hPa shear (lower) and the 100–150 hPa shear (lower). While multiple GJ cases show consistently enhanced values for most of these parameters, none of these are statistically significant at the 99% level when compared to the single GJ cases instead of the null cases. The $SH_{150–100}$ difference is significant at the 95% level.

3.9. Robustness

While the above statistics are robust, with large Cohen's d values and *p*-values of the Welch *t*-test well beyond the 99% significance level (<<0.01), the selection of ERA5 profiles involved human choices seeking a compromise between proximity in time and space and conditions supporting convection.

Here we use another methodology to produce alternative profiles with minimal human intervention. ERA5 profiles are taken at fixed locations in northern Colombia: (A) 10°N 74.5°W, (B) 9°N 74.5°W, and (C) 8°N 75.5°W, at 0000, 0300, 0600 and 0900 UTC for each GJ and null event within about 1° of one of these locations. Two "proximity profiles" are then assigned to each case based on proximity in time and space, for example, location C at 0300 and 0600 UTC, closest to the manually selected time and location of the original method and actual event. In addition, for this example, profiles of all times in locations A and B, as well as 0000 and 0900 UTC at location C, are grouped as "non-proximity" profiles (10 per case). This enables a complementary view on the sensitivity of the results to the proximity sounding and the regional and temporal performance of the parameters.

A selection of the statistical results of this procedure is shown in Table 7. The table separates the proximity profiles and the non-proximity profiles far from the event in space or time. The Cohen's d column shows that the warm/cold cloud parameters in proximity profiles still reveal the same tendencies as hand-picked profiles. The values are only slightly reduced. In contrast, the parameters $Z_{-10°C}$, $DZ_{-10\ -50°C}$ and WCDRAT show significant separation between GJ and null cases even in *non*-proximity profiles, keeping similar mean values, indicating that these conditions occur across a wide region, likely associated with synoptic scale weather patterns.

For instability-related parameters CAPE, CIN and DD $\Delta\theta_{ES\ 950}$ the proximity profiles still reveal the same tendencies as the original method, while the non-proximity profiles do not. As expected, CAPE and CIN are weaker or less favorable for convection than in the original hand picked profiles.

Table 5
Mean values, statistical significance and effect size for parameters of the wind environment for the GJ cases and null cases by region.

Parameter	N Colombia		W Colombia		Carib. Sea	p-value			Cohen's d		
	Null (61)	GJ (20)	Null (22)	GJ (12)	GJ (17)	NCol	WCol	All	NCol	WCol	All
$SH_{150–100}$ (m s^{-1})	11.0	8.02	10.5	7.40	9.82	0.03	0.08	0.03	0.51	0.58	0.40
$SH_{300–150}$ (m s^{-1})	10.0	7.61	9.51	8.57	8.30	0.02	0.59	0.04	0.50	0.16	0.34
$SH_{925–750}$ (m s^{-1})	**8.40**	**6.56**	4.60	5.01	4.36	**1e-3**	0.52	**2e-3**	**0.67**	0.25	0.53
$MW_{0–6}$ (m s^{-1})	**3.51**	**2.55**	2.24	1.90	4.75	**9e-3**	0.17	0.72	**0.65**	0.47	0.07
$SRW_{200–100}$ (m s^{-1})	9.29	8.93	**8.42**	**6.27**	9.32	0.73	**1e-2**	0.40	0.09	**0.85**	0.14
$SRW_{1000–700}$ (m s^{-1})	**3.74**	**2.89**	2.56	2.61	2.39	**8e-5**	0.84	**1e-4**	**0.81**	0.07	**0.63**
$MSH_{1000–600}$ (10^{-3} s^{-1})	**4.18**	**3.52**	3.19	3.36	3.15	**4e-3**	0.50	**4e-3**	**0.76**	0.24	0.50

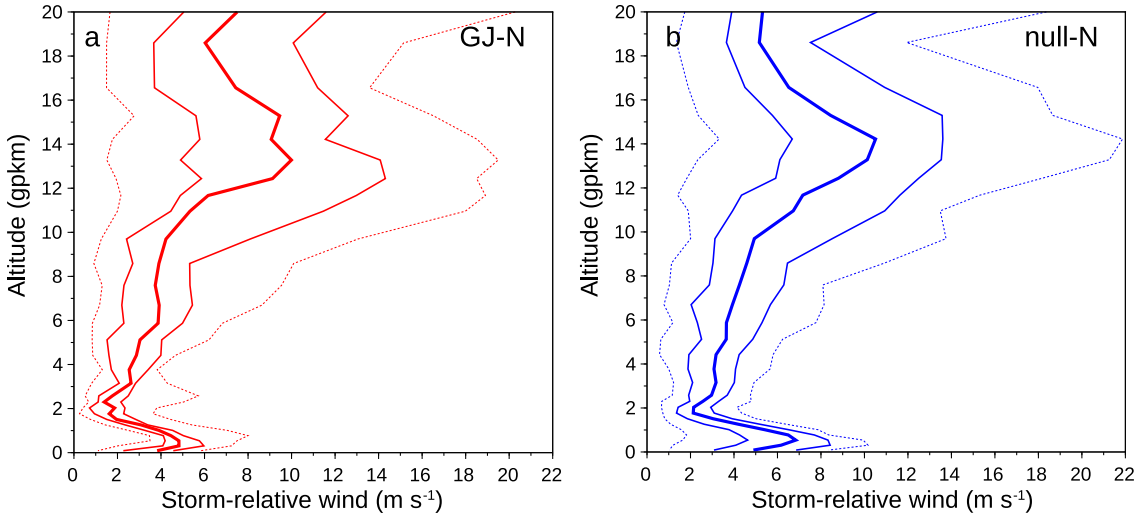

Fig. 5. Storm-relative wind speed with altitude for gigantic jet (a) and null cases (b) over northern Colombia, represented by the 5th, 25th, 50th (thick line), 75th and 95th percentiles of the distribution.

Table 6
Effect size for various parameters for 14 multiple-GJ cases and 35 single-GJ cases, compared to 83 null cases. Minus signs are added to indicate when parameter values are lower than those of the null cases.- The last column shows the enhancement in absolute effect size for multiple GJ compared to single GJ cases.

Parameter	Cohen's d		
	Multi GJ (14)	Single GJ (35)	Difference Multi to Single
$Z_{-10°C}$ (m)	**0.87**	0.42	+107%
$WCD_{-10°C}$ (m)	**1.05**	**0.89**	+18%
$DZ_{-10\ -50°C}$ (m)	**−1.06**	**−0.98**	+8%
WCDRAT (ratio)	**1.41**	**1.18**	+19%
$CON_{-10°C}$ (g kg^{-1})	**0.89**	**0.65**	+36%
$CON_{-10\ -30°C}$ (g kg^{-1})	−0.51	**−0.56**	−9%
WCCRAT (ratio)	**0.97**	**0.88**	+10%
WCCRAT*EL	**1.64**	**1.31**	+25%
$MSH_{1000–600}$ (10^{-3} s^{-1})	**−0.71**	−0.39	+82%
$SH_{150–100}$ (m s^{-1})	**−0.70**	−0.27	+159%
MPL-EL (km)	**−0.67**	**−0.53**	+26%
DD $\Delta\theta_{ES\ 950}$ (K)	**0.56**	**0.70**	−14%

The $SRW_{1000–700}$ performance remained stable, while $MSH_{1000–600}$ performed better (Cohen's d from 0.76 to 0.95) on the alternative proximity profiles.

3.10. *Effect of profile time*

According to the time histogram in **Fig. S1**, GJ profiles are distributed later during the night than null profiles over northern Colombia. Profiles tend to become more stable as the lower levels cool during the night, affecting many of the parameters which have been reported here as significant for GJ production (e.g. lapse rate, cloud base height, CAPE). As stabilization occurs every night, one may ask to which extent the results may be biased. To investigate this, GJ and null proximity profiles obtained with the method described in the previous section are compared at 3-h intervals throughout the night. Fig. 6 shows the time dependency of the WCCRAT parameter and its constituents, $CON_{-10°C}$ and $CON_{-10\ -30°C}$. At any given 00–03–06–09 UTC time GJ events are clearly associated with higher WCCRAT values than null cases ($p < 0.01$ except for 09 UTC). However, the overall increase with time leads to the situation that null cases later in the night occur with similar WCCRAT values as the GJ cases several hours earlier. This complicates the use of the parameter in forecasting. The cause of the trend is mainly due to an

Table 7
Mean value and effect size for various parameters using the fixed location approach for profile selection, for 20 gigantic jet cases and 57 null cases over northern Colombia (2 proximity profiles and 10 non-proximity profiles per case). The *p*-value is calculated based on the number of cases (not profiles).

Parameter	Proximity		Non-proximity		p-value		Cohen's d	
	Null 57 (114)	GJ 20 (40)	Null 57 (570)	GJ 20 (200)	Proximity	Non-proximity	Proximity	Non-proximity
$Z_{-10°C}$ (m)	6668	6739	6664	6741	0.02	0.01	0.61	0.62
$WCD_{-10°C}$ (m)	5770	6028	5787	5933	**3e-5**	0.04	**0.98**	0.53
$DZ_{-10\ -50°C}$ (m)	5430	5336	5421	5330	**4e-3**	**3e-3**	**0.81**	**0.75**
WCDRAT (ratio)	1.06	1.13	1.07	1.11	**3e-6**	**1e-3**	**1.25**	**0.82**
$CON_{-10°C}$ (g kg^{-2})	12.11	12.48	11.99	12.32	0.01	0.05	0.53	0.48
$CON_{-10\ -30°C}$ (g kg^{-2})	3.80	3.52	3.64	3.57	**1e-4**	0.22	**0.97**	0.28
WCCRAT (ratio)	3.20	3.56	3.30	3.47	**5e-6**	0.02	**1.45**	0.63
WCCRAT*EL	44.80	48.15	43.87	47.58	**5e-3**	**2e-3**	**0.72**	**0.77**
DD $\Delta\theta_{ES\ 950}$ (K)	−32.0	−21.9	−30.4	−27.0	**2e-6**	0.21	**1.09**	0.32
CAPE (J kg^{-1})	1587	1113	1223	1279	**5e-4**	0.72	**0.78**	0.09
CIN (J kg^{-1})	−40	−36	−60	−47	0.53	0.13	0.14	0.36
RH_{925} (%)	77.6	87.2	76.6	78.6	**3e-6**	0.47	**1.07**	0.18
SD (kg m^{-2})	21.8	16.7	22.2	20.3	**6e-5**	0.26	**0.94**	0.28
$SRW_{1000–700}$ (m s^{-1})	3.92	3.13	3.59	3.36	**6e-4**	0.38	**0.82**	0.22
$MSH_{1000–600}$ (10^{-3} s^{-1})	4.38	3.54	4.14	3.92	**2e-4**	0.39	**0.94**	0.22
$SH_{150–100}$ (m s^{-1})	10.69	8.31	11.19	9.48	0.08	0.22	0.41	0.30
MPL-EL (km)	3.42	3.45	3433	3391	0.81	0.78	0.06	0.07

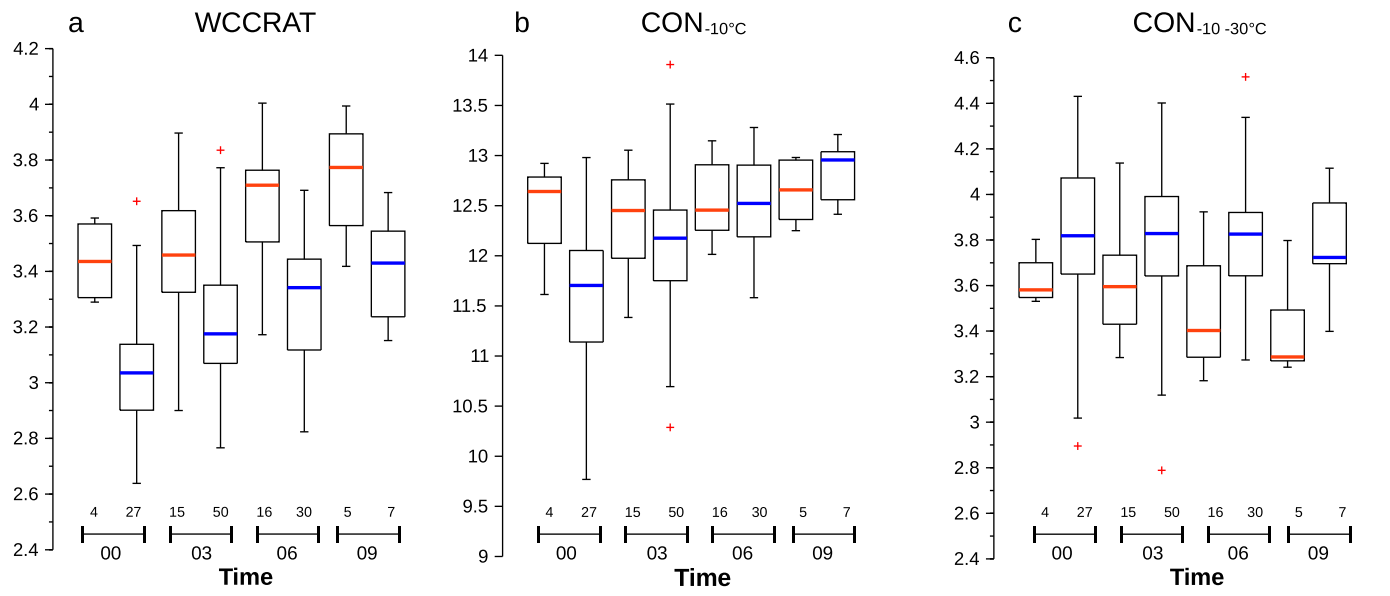

Fig. 6. Distribution of WCCRAT, $CON_{-10°C}$ and $CON_{-10\ -30°C}$ parameters compared by time intervals (UTC) in proximity profiles for gigantic jet cases (red) and null cases (blue) in northern Colombia. (For interpretation of the references to color in this figure legend, the reader is referred to the web version of this article.)

increase in $CON_{-10°C}$ during the night. As Fig. 6 was made using proximity profiles only, nocturnal trends are not captured correctly, as each time bin contains a different set of cases. If we include non-proximity profiles to help understand how the parameters change during the night (not shown), we find an increasing trend in $CON_{-10°C}$ both in null and GJ cases as most important driver of the trend in WCCRAT. The increase is due to a slight increase of boundary layer mixing ratio (stronger in area B), together with a slight decrease in Z_{-10C} and a decrease in θ_E (parcel temperature) by nocturnal cooling which both reduce r_{-10C}. $CON_{-10\ -30°C}$ (much like Lifted Index) stays relatively constant as r_{-10C} and r_{-30C} are affected about equally by these changes. The observation from Fig. 6b that $CON_{-10°C}$ stays rather constant in GJ proximity profiles suggests local or temporary enhancement of this parameter in GJ cases with respect to the typical nocturnal trend.

Similar figures could be plotted for WCDRAT, $WCD_{-10°C}$ and $CCD_{-10\ -50°C}$, even though the latter reflects the mid-upper level ambient temperatures while $CON_{-10\ -30°C}$ is a parcel parameter.

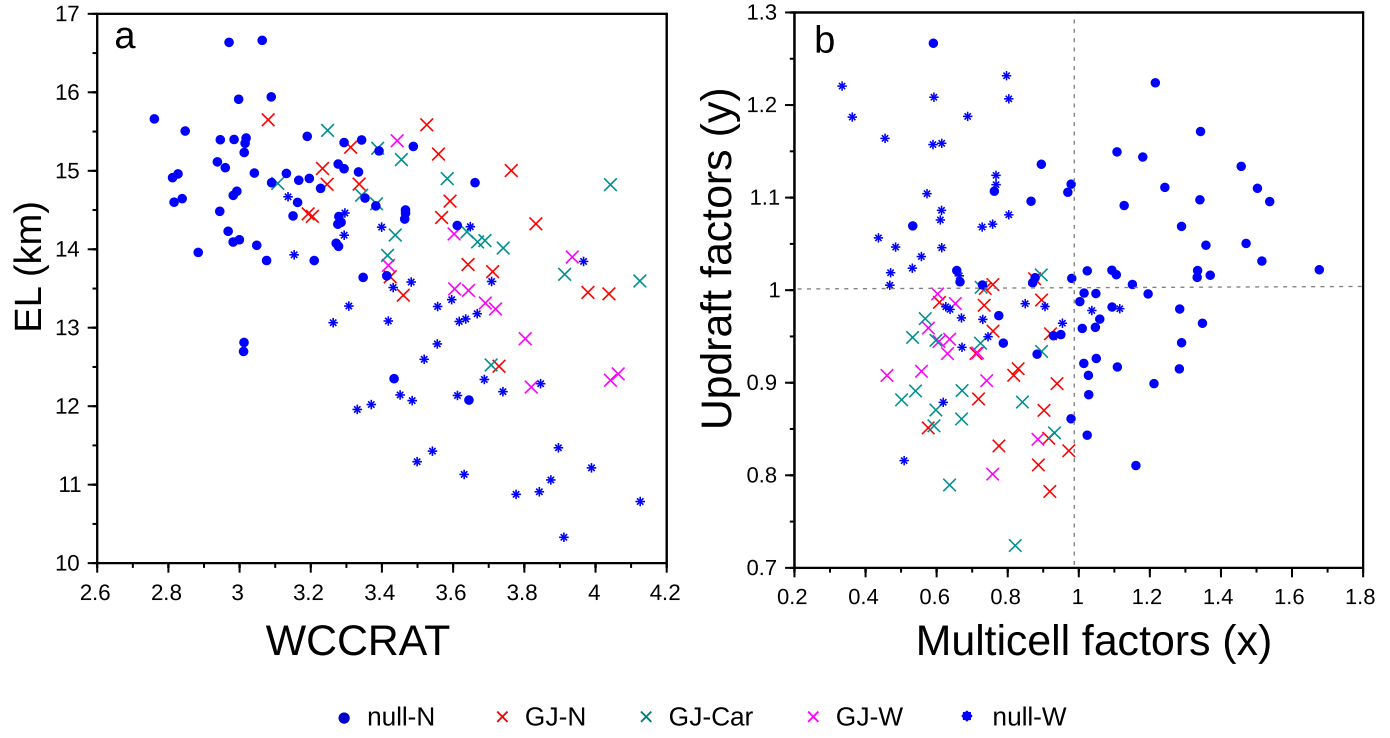

Fig. 7. (a) Parameter space of WCCRAT and EL height for gigantic jet and null cases. (b) Parameter space for two composite parameters that represent downdraft buoyancy and low-level storm-relative winds (x) and updraft buoyancy and warm cloud parameters (y), described in the text.

4. Discussion

4.1. Parameter space and forecasting

In the previous sections, the microphysical, instability, downdraft and low-level shear parameters showed potential for separating between GJ and null cases. However, they also highlighted differences between northern and western Colombia, such that no single parameter could work well in the forecasting of gigantic jets across all regions. In northern Colombia, the null cases had lower WCCRAT and higher CAPE, DD and $SRW_{1000–700}$ values than the GJ cases, while in western Colombia the null cases show values of those parameters indistinguishable from the GJ cases. We explored the parameter space of several independent parameters, and noted one factor that appears to make an important difference for distinguishing between GJ and null cases in western Colombia. Fig. 7a shows an example of the parameter space of WCCRAT and the equilibrium level height. It can be noted that the markers for western Colombia null cases indicate lower EL heights for similar values of WCCRAT as for the GJ cases in that region. It shows that a variable without a statistically significant difference between the means of the GJ and null populations can still be a prerequisite condition. As its denominator $CON_{-10\ -30°C}$ is a function of parcel temperature relative to ambient temperature, WCCRAT tends to increase with decreasing CAPE values within the tropics, where the isotherm altitudes and mixed layer parcel properties do not vary over a large range. Combining WCCRAT with EL height guarantees sufficient upper level buoyancy and cloud top altitude.

Two of the parameters that separate GJ and null cases very well in northern Colombia relate to the cold pool strength and vertical wind shear in the low levels, of which the null cases show the highest values. This combination suggests more effective convective updraft triggering processes by outflow boundaries (e.g. Rotunno et al., 1988) leading to multicell storms, which may be detrimental to the production of gigantic jets. In our estimation, the majority of null cases, but few of the GJ producing storms, were of multicell type. In addition, the observation that gigantic jets are globally most often observed over tropical seas (Chern et al., 2014) is consistent with these parameters. The cooler low level air over sea reduces cold pool strength, instability and cloud base height, while low-level shear tends to be weaker because of reduced surface friction, absence of topography-induced flow patterns and lack of thermal wind in the tropics.

Plotting these "multicell factors" on the x-axis, and some of the "updraft factors" on the y-axis, Fig. 7b reveals a section of the parameter space occupied mostly by GJ profiles with few null profiles. Here we used $x = \mathrm{sqrt}(SRW_{1000–700} * DD\ \Delta\theta_{ES\ 950})$, normalized by 4 m s^{-1} and 25 K respectively, and $y = DZ_{-10\ -50°C} / (WCCRAT*Z_{EL})$ normalized by 5300 m, 3.5 and 13,000 m respectively, such that the lines $x = 1$ and $y = 1$ separate well the GJ and null data points.

A multivariate logistic regression (e.g. Ranganathan et al., 2017) was used to construct a forecasting index. The index indicates a probability of gigantic jets on the condition that storms occur. We chose a set of 5 variables with minimal collinearity and component p-values <0.01, consisting of $WCCRAT*Z_{EL}$, $MSH_{1000–600}$, $Z_{-50°C}$, (DD) $\theta_{e\ 500}$ and $SH_{150–100}$ with weights and test scores included in the Supplementary Information. On this data set, the regression function scores a Cohen's d of 1.92 overall for GJ versus null, 2.10 for multi-GJ to null overall, and 0.57 for multi-GJ to single GJ (improved, but not significant, $p = 0.07$). Examples of forecast maps are included in the Supplementary Information. However, model forecasts may have difficulties in correctly representing the convective environment and precipitation, affecting the index. The probability range resulting from the logistic regression is inflated as the limited selection of data does not reflect the true ratio of null to GJ nights.

4.2. Physical understanding

By the use of a large dataset of null cases in addition to the 61 GJ cases, this statistical analysis of the meteorological environment of gigantic jet parent storms is able to determine the ambient parameters relevant to the GJ production. In this study, we found no statistical evidence for enhanced vertical wind shear or storm-relative winds at the cloud top, suggested by Lazarus et al. (2015, 2021) and, for an unusual winter GJ case, van der Velde et al. (2010). Although we cannot exclude that shallow shear maxima were not sampled by the 25 hPa interval ERA5 data we used, there are in fact modest signals that stronger 150–100 hPa wind shear is more common in null cases than in GJ cases. We also found that gigantic jets associate with less CAPE, in the general range of 500–2200 J kg^{-1}, without significant differences in EL and MPL heights and a slightly reduced overshoot size (MPL-EL). Similarly, Lazarus et al. (2021) reported a limited tropopause penetration in tropical cyclone GJ cases. On the other hand, a larger overshooting top has been suggested as a favorable factor that helps direct gigantic jets vertically out of the cloud (Boggs et al., 2018).

On the other hand, the null cases in northern Colombia with a large CAPE also have steeper lapse rates and higher cloud bases, and therefore enhanced outflow strength and reduced warm cloud depth, which are found to be more strongly associated with no GJ production. A direct effect of stronger CAPE may be the turbulent fragmentation of the charge distribution, discharged by frequent small intracloud flashes (Bruning and MacGorman, 2013) instead of having a single contiguous charge layer which may be needed to supply a gigantic jet its energy.

As mentioned in Section 4.1, colder downdrafts and stronger vertical wind shear in the low levels act together as trigger for new updraft initiation. This helps generate large multicell storms and mesoscale convective systems (MCS). In our data set, a number of null cases featured sprites, which are usually produced by MCS or decaying storm clusters above the stratiform precipitation region. In our experience, the GJ-producing cells tend to be rapidly growing discrete cells, with an easily tracked cloud top evolution on satellite images, while many null cases include strong multicell clusters with smaller embedded overshooting tops. Whenever GJ occur quasi-simultaneously with sprites, they are usually negative sprites (van der Velde et al., 2019, supp. Info.), which tend to be produced by relatively young convective cells in Colombia. However, additional study is needed to document storm type and evolution associated with gigantic jets. Multicells may have unfavorable interference between adjacent updraft and downdraft processes, and lack a singular growth-decay cycle. Additionally, a warmer (less negatively buoyant) downdraft will not cut off the updraft as quickly from its inflow air supply, so that the cell updraft can peak a bit longer. While it is possible that the preference for weak downdraft potential is a side effect of the optimal warm cloud and mixed phase parameters which are correlated via the temperature lapse rate, the differences in the warm cloud values between GJ and null cases are marginal in comparison. When weak low-level wind shear is combined with a weak cold pool, the updraft inflow and generated rain drops may be better vertically collocated, which benefits the efficiency of coalescence, resulting possibly in more large supercooled drops entering the mixed phase region instead of falling out the sides of the updraft. However, such vertical collocation by upright updrafts should occur for any balanced, stronger combinations of low-level shear and cold pool strength (Rotunno et al., 1988). Investigating this by plotting cold pool strength against 975–800 hPa mean shear (Fig. S3), a possible optimal zone can be noted where GJ cases concentrate, but few null cases. It must be considered, however, that GJ-producing (and null) cells were not necessarily triggered by interaction with outflow from adjacent convective cells.

A strong performance was found for parameters related to the warm cloud depth and condensation (particularly those relative to the −10 °C level), especially when combined with properties of the mixed phase region. Much of this comes down to the slightly warmer mid levels in GJ

cases, although the difference in temperature itself (or altitude of the −10 °C level) is not statistically significant and the LCL height on its own offers only modest separation. It is the combination of both that improves the GJ-null separation. Similarly, we found that the vertical distance between −10 °C and − 50 °C isotherms is smaller during GJ nights, even when sampled in time and space away from the actual thunderstorm. This parameter may be associated with with modification of lapse rates by vertical motion at the mesoscale or synoptic scale or as a result of convective activity. By studying reanalysis or forecast maps of this parameter it may be understood better how weather systems create a favorable environment for gigantic jet-producing storms.

The deep warm cloud preference explains why GJs are restricted to tropical airmasses. The events and null cases in western Colombia revealed an additional condition that needs to be met. A large fraction of null cases in that region, even while typically producing strong lightning activity throughout the night, under otherwise favorable conditions for gigantic jets, featured lower EL heights. Fig. 7a suggests that as WCCRAT increases, the lowest EL height at which gigantic jets are produced decreases. This indicates a possible relation between WCCRAT and the negative potential the leader may acquire, as a higher negative potential is required for a leader to jump from a lower altitude cloud top to the ionosphere.

The observation that GJ production correlates with the highest warm cloud parameter values, along with modest instability in the mixed phase region, suggests a crucial role for particular microphysical processes in the cloud in enabling gigantic jet production. Although limited by the current scientific understanding of the physics of cloud and precipitation particles and their electrification, we discuss here the possible implications of warm cloud processes to GJ production. An visual summary of this discussion is provided in Fig. S4.

Warm rain coalescence processes convert cloud droplets into growing, precipitation-sized droplets. The more time droplets reside in this regime and collide with others, the larger they grow, therefore WCD regulates its efficiency. Other factors as high liquid water content, low entrainment of dry air and low aerosol content (e.g. Williams et al., 2005) also contribute. If WCD is shallow, predominantly small cloud droplets and drizzle droplets are produced that are transported by the updraft up into the mixed phase region (−10 °C to −30 °C), where some will freeze heterogeneously by contact with ice or ice nucleation particles; others will evaporate and sublimate back onto ice cystals; and part will collide and freeze onto ice particles (riming). A secondary ice production (SIP) mechanism (e.g. Field et al., 2017; Korolev and Leisner, 2020) such as the rime splintering process (Hallett-Mossop) then multiplies the ice particle numbers. Ice particles will experience a strong growth by riming thanks to the high cloud droplet concentration.

On the other end of the spectrum, a large WCD generates larger rain drops at the cost of small ones and cloud droplets. Many of the heavier drops fall out of the updraft before reaching the mixed phase region, but those that make it can heterogenously freeze and become riming ice particles. Large supercooled drops tend to shatter off ice shells upon freezing (another form of SIP) which multiplies the ice number concentration. However, the reduced concentration of small cloud and drizzle droplets compared to that of larger particles, which become riming targets, makes for a low rime accretion rate. Additionally, the reduction in adiabatic condensation within the mixed phase region (−10 °C to −30 °C) in profiles associated with gigantic jets suggests decreased new supercooled cloud droplet production, hence maintained low rime accretion rates in this temperature region.

Although enhanced warm rain processes may reduce the efficiency of mixed phase electrification processes in storms (e.g. Williams et al., 2005; Morales Rodriguez, 2019), the detected cloud-to-ground lightning (CG) activity in our Colombian GJ-producing storms does not give us the impression that electrification was reduced to a low level. We confirmed in one GJ-producing storm moderate optical flash rates of 8 per minute in the 10-min interval surrounding a GJ event (on 3 June 2020), higher than the case discussed by Soula et al. (2011). In fact, a not insignificant fraction of GJ parent storms even produces strokes with high negative currents (< −50 kA) every few minutes (or less). Fig. S5 shows two examples. It is known that strong negative sprite-producing strokes occasionally occur in the period (minutes to half an hour) around gigantic jets (Boggs et al., 2016; van der Velde et al., 2019). Those strokes apparently do not deplete the negative charge region appreciably. During our optical campaigns in Colombia it was noted that strong strokes are typically of the bolt-from-the-blue type coming from the side of the updraft tower (Krehbiel et al., 2008). We see a need for more thorough research into the lightning activity aspects of GJ producing storms in order to recognize the possible signals of a favorable charge distribution.

We propose that low rime accretion rates or enhanced secondary ice production processes (or both) resulting from the high warm cloud/mixed phase parameters are key to the excess negative charging needed for tropical gigantic jet initiation. There is support from natural and laboratory observations that rime accretion rates are capable of changing the polarity of charging. Conditions where WCD is reduced to only 1000–2000 m have been associated with anomalous thunderstorms in the central USA that produce predominantly positive CG flashes (Carey and Buffalo, 2007; Eddy et al., 2021) and very high total flash rates (Fuchs et al., 2015). Under this condition, the rime accretion rate is thought to reach such high levels that polarities of the graupel and ice charges are reversed in the mixed phase region, in agreement with laboratory studies. Those studies, summarized by Mansell et al. (2005) and Emersic and Saunders (2010), not only indicate inverted polarity charging at high rime accretion rate, but also at very *low* rime accretion rate (or liquid cloud water content, or supersaturation). In another laboratory experiment, Avila et al. (1998) observed that the riming ice in the regime warmer than −15 °C is more likely to charge negatively if larger cloud droplets are present. This suggests that the enhanced warm cloud coalescence conditions for gigantic jets could support a lower *negative* charge region instead of the usual lower positive, and thus could offer a deeper reservoir of negative charge - if the graupel in the colder mixed phase region maintains a normal negative charge polarity. At very low riming rates graupel may start to charge positively in that temperature region, according to the summary by Emersic and Saunders (2010).

The uncertainties about microphysical processes and their effects on the charging make it difficult to explain how the required negative imbalanced charge structure (Krehbiel et al., 2008) could emerge. However, the imbalanced charge configuration only needs to exist for a short time during the evolution of a storm, on the order of convection and electrification time scales (<10 min). Cases with multiple jets show they often cluster within just a few minute intervals (Soula et al., 2011; Liu et al., 2015). It is plausible that the storm initially develops a normal dipolar or tripolar charge configuration, producing intracloud and -CG flashes. A weakening of the updraft could lower the rime accretion rate by reduced concentrations of cloud droplets. This should first occur in the lower parts of the cloud, and therefore may affect the lower charge region before the central and upper regions. This makes graupel gain negative charge in the warm part of the mixed phase region, while graupel in the cold region will slowly acquire positive charge but will still be mostly negatively charged. The upper positive charge region may become diluted by the arrival of negatively charged ice crystals from below, while cloud top divergence disperses positive charge in the highest regions (Soula et al., 2011). This could introduce a brief period in which a lightning flash can gain significant negative potential and exit the cloud top as a gigantic jet. A further benefit could be provided by a new updraft surge, which would reinstate the default charging polarity, and lift existing negatively charged graupel. A new concentration of positively charged small ice particles on top of the bolstered negative charge region would then help the discharge grow upwards through a weak upper positive charge region. Such surge would need to affect the charged precipitation regions formed by the previous updraft, instead of creating new updrafts next to existing ones as in multicell storms. Some

evidence for convective surges associated with gigantic jets was presented by Meyer et al. (2013). A possible supportive observation for our hypothesis is the evolution of graupel reported by Lazarus et al. (2015), using dual-polarimetric weather radar. Two isolated small jets each occurred shortly after a corresponding sharp drop in graupel at 9.4 km (~ −30 °C), while a cluster of 5 events including gigantic jets occurred shortly after the graupel volume sharply increased again after a temporary minimum.

More evidence for the microphysical responses to environment parameters suggested here could be sought in observations of the ice water path, using weather radar (e.g. Kalina et al., 2017) or satellite-based radar instruments, to confirm reduced small ice particle content in the upper regions of the cloud and increased large ice particle content in the mixed phase region. Eventually, to better understand the sensitivity to environmental factors like the ones we reported, a future study using an idealized cloud model can help visualize and understand their effects on the evolution of microphysical particle distributions responsible for the electrification.

5. Conclusion

This study is the first to compare the meteorological environment for a large data set of gigantic jets against a comparable number of null case storms. It is because of the reference provided by the null events that one is able to tell whether certain parameters were enhanced during GJ events.

Our main finding using ERA5 data is that GJ nights features cooler temperatures in the low levels, even compared by different hours of the night, combined with slightly warmer mid levels and slightly cooler high levels. This sets up a lower cloud base, greater warm cloud depth (to the −10 °C level) and lower instability (Lifted Index and CAPE). Weaker downdraft buoyancy and weak storm-relative inflow winds in the 1000–700 hPa (<3 km MSL) layer work against multicell storm morphology and reduce the impact of outflow air on updraft longevity. There appears to be a minimum requirement of the cloud top height, with an EL height of about 12–13 km depending on the other parameters. A wide range of upper level shear values occurs in GJ and null categories in all three regions, suggesting this parameter plays no clear role in gigantic jet production by tropical thunderstorms. Therefore, the hypotheses about the influence of strong vertical wind shear and higher overshooting cloud tops are not supported by this study.

Interestingly, the parameters that apparently support an exceptional electrical configuration are generally considered less favorable for vigorous and sustained deep convection. The observed statistically significant parameters are characteristic of the "moist tropical paradigm" (Lazarus et al., 2015) itself, without needing additional factors to produce gigantic jets. The rareness of warm cloud parameter values as $WCD_{-10°C} > 5800$ m or $CON_{-10°C} > 12$ g kg^{-1} in mid-latitude thunderstorm environments explains why gigantic jets are typically not observed there, in addition to other factors.

We attribute the required negatively imbalanced vertical charge structure to changes in the rime accretion rate and secondary ice production by the increased warm rain coalescence processes and decreased mixed phase buoyancy, likely modulated by the evolution of the storm updraft. Additional studies are needed to unravel how the tropical conditions quantified here precisely affect the dynamical, microphysical and electrical processes during the life of a thunderstorm.

Data availability

Data for this study has been deposited in the Zenodo scientific repository: https://zenodo.org/record/4705233

CRediT authorship contribution statement

Oscar A. van der Velde: Conceptualization, Methodology, Software, Formal analysis, Investigation, Data curation, Writing – original draft, Writing – review & editing, Visualization. **Joan Montanyà:** Funding acquisition. **Jesus A. López:** Resources, Investigation.

Declaration of Competing Interest

The authors declare that they have no known competing financial interests or personal relationships that could have appeared to influence the work reported in this paper.

Acknowledgments

We thank David Romero and Daniel Aranguren for servicing the San Andrés island camera system, John Taborda and his students for hosting and servicing the Santa Marta camera system, Juan Diego Pulgarin and Adriana Arango for hosting and servicing the Barranquilla camera system, Camilo Younes and his students for hosting and servicing the Manizales camera system, and Albert Martis and Haime Pieter for hosting and servicing the Curaçao camera system. ERA5 data was obtained via the Copernicus Climate Change Service (C3S). Data has been obtained and curated during subsequent projects funded by the Spanish Ministry of Economy and European Regional Development Fund (FEDER): AYA2009-14027-C05-05, AYA2011-29936-C05-04, ESP2013-48032-C5-3-R, ESP2015-69909-C5-5-R, ESP2017-86263-C4-2-R, PID2019-109269RB-C42.

Appendix A. Supplementary data

Supplementary data to this article can be found online at https://doi.org/10.1016/j.atmosres.2022.106316.

References

Albrecht, R.I., Goodman, S.J., Buechler, D.E., Blakeslee, R.J., Christian, H.J., 2016. Where are the lightning hotspots on Earth? Bull. Am. Meteorol. Soc. 97 (11), 2051–2068.

Aranguren, D., López, J., Inampués, J., Torres, H., Betz, H.D., 2014. Cloud-to-ground lightning activity in Colombia and the influence of topography. J. Atmos. Solar-Terrestrial Phys. https://doi.org/10.1016/j.jastp.2016.08.010.

Arnone, E., Bór, J., Chanrion, O., et al., 2020. Climatology of transient luminous events and lightning observed above Europe and the Mediterranean Sea. Surv. Geophys. 41, 167–199. https://doi.org/10.1007/s10712-019-09573-5.

Avila, E., Caranti, G., Castellano, N., Saunders, C., 1998. Laboratory studies of the influence of cloud droplet size on charge transfer during crystal-graupel collisions. J. Geophys. Res. 103 (D8), 8985–8996. https://doi.org/10.1029/97JD03115.

Boggs, L.D., Liu, N., Splitt, M., Lazarus, S., Glenn, C., Rassoul, H., Cummer, S.A., 2016. An analysis of five negative sprite-parent discharges and their associated thunderstorm charge structures. J. Geophys. Res. Atmos. 121, 759–784. https://doi.org/10.1002/2015JD024188.

Boggs, L.D., et al., 2018. Thunderstorm charge structures producing gigantic jets. Sci. Rep. 8, 18085. https://doi.org/10.1038/s41598-018-36309-z.

Bolton, D., 1980. The computation of equivalent potential temperature. Mon. Weather Rev. 108, 1046–1053. https://doi.org/10.1175/1520-0493(1980)108<1046:TCOEPT>2.0.CO;2.

Bruning, E.C., MacGorman, D.R., 2013. Theory and observations of controls on lightning flash size spectra. J. Atmos. Sci. 70, 4012–4029.

Carey, L.D., Buffalo, K.M., 2007. Environmental control of cloud-to-ground lightning polarity in severe storms. Mon. Weather Rev. 135 (4), 1327–1353.

Chen, A.B., et al., 2008. Global distributions and occurrence rates of transient luminous events. J. Geophys. Res. 113, A08306.

Chern, J.L., Wu, A.M., Lin, S.F., 2014. Globalization extension of transient luminous events from FORMOSAT-2 observation. Acta Astron. 98, 64. https://doi.org/10.1016/j.actaastro.2014.01.014.

Cummer, S.A., et al., 2009. Quantification of the troposphere-to-ionosphere charge transfer in a gigantic jet. Nat. Geosci. 2, 617. https://doi.org/10.1038/ngeo607.

Delacre, M., Lakens, D., Leys, C., 2017. Why psychologists should by default use welch's t-test instead of student's t-test. Int. Rev. Soc. Psychol. 30 (1), 92–101. https://doi.org/10.5334/irsp.82.

Dunion, J.P., 2011. Rewriting the climatology of the Tropical North Atlantic and Caribbean Sea Atmosphere. J. Clim. 24 (3), 893–908. https://doi.org/10.1175/2010JCLI3496.1.

Eddy, A.J., MacGorman, D.R., Homeyer, C.R., Williams, E., 2021. Intraregional comparisons of the near-storm environments of storms dominated by frequent positive versus negative cloud-to-ground flashes. Earth Space Sci. 8, e2020EA001141 https://doi.org/10.1029/2020EA001141.

Emersic, C., Saunders, C.P.R., 2010. Further laboratory investigations into the relative diffusional growth rate theory of thunderstorm electrification. Atmos. Res. 98 (2-4) https://doi.org/10.1016/j.atmosres.2010.07.011.

Field, P.R., et al., 2017. Secondary ice production: current state of the science and recommendations for the future. Meteorol. Monogr. 58, 7.1-7.20. https://doi.org/10.1175/AMSMONOGRAPHS-D-16-0014.1.

Fuchs, B.R., Rutledge, S.A., Bruning, E.C., Pierce, J.R., Kodros, J.K., Lang, T.J., MacGorman, D.R., Krehbiel, P.R., Rison, W., 2015. Environmental controls on storm intensity and charge structure in multiple regions of the continental United States. J. Geophys. Res. Atmos. 120, 6575–6596. https://doi.org/10.1002/2015JD023271.

Hersbach, H., Bell, B., Berrisford, P., et al., 2020. The ERA5 global reanalysis. Q. J. R. Meteorol. Soc. 146, 1999–2049. https://doi.org/10.1002/qj.3803.

Kalina, E.A., Matrosov, S.Y., Cione, J.J., Marks, F.D., Vivekanandan, J., Black, R.A., Hubbert, J.C., Bell, M.M., Kingsmill, D.E., White, A.B., 2017. The ice water paths of small and large ice species in hurricanes arthur (2014) and Irene (2011). J. Appl. Meteorol. Climatol. 56 (5), 1383–1404. https://doi.org/10.1175/JAMC-D-16-0300.1.

Korolev, A., Leisner, T., 2020. Review of experimental studies of secondary ice production. Atmos. Chem. Phys. 20, 11767–11797. https://doi.org/10.5194/acp-20-11767-2020.

Krehbiel, P.R., et al., 2008. Upward electrical discharges from thunderstorms. Nat. Geosci. 1, 233–237. https://doi.org/10.1038/ngeo162.

Lakens, D., 2013. Calculating and reporting effect sizes to facilitate cumulative science: a practical primer for t-tests and ANOVAs. Front. Psychol. https://doi.org/10.3389/fpsyg.2013.00863.

Lazarus, S.M., Splitt, M.E., Brownlee, J., Spiva, N., Liu, N., 2015. A Thermodynamic, kinematic and microphysical analysis of a jet and gigantic jet-producing Florida thunderstorm. J. Geophys. Res. Atmos. 120, 8469–8490. https://doi.org/10.1002/2015JD023383.

Lazarus, S.M., Chiappa, J., Besing, H., Splitt, M.E., Riousset, J.A., 2021. Distinguishing characteristics of the tropical cyclone gigantic jet environment. J. Atmos. Sci. 78 (9), 2741–2761.

Liu, N., et al., 2015. Upward electrical discharges observed above tropical depression Dorian. Nat. Commun. 6, 5995. https://doi.org/10.1038/ncomms6995.

López, J.A., et al., 2019. Charge structure of two tropical thunderstorms in Colombia. J. Geophys. Res. Atmos. 124, 5503–5515. https://doi.org/10.1029/2018JD029188.

Lu, G., et al., 2011. Lightning development associated with two negative gigantic jets. Geophys. Res. Lett. 38, L12801. https://doi.org/10.1029/2011GL047662.

Mansell, E.R., MacGorman, D.R., Ziegler, C.L., Straka, J.M., 2005. Charge structure and lightning sensitivity in a simulated multicell thunderstorm. J. Geophys. Res. 110, D12101. https://doi.org/10.1029/2004JD005287.

Manzato, A., Morgan, G.M., 2003. Evaluating the sounding instability with the lifted parcel theory. Atmos. Res. 67–68, 455–473.

Mapes, B.E., Warner, T.T., Xu, M., Negri, A.J., 2003. Diurnal patterns of rainfall in Northwestern South America. Part I: Observations and context. Mon. Weather Rev. 131 (5), 799–812.

Meyer, T.C., Lang, T.J., Rutledge, S.A., Lyons, W.A., Cummer, S.A., Lu, G., Lindsey, D.T., 2013. Radar and lightning analyses of gigantic jet-producing storms. J. Geophys. Res. Atmos. 118, 2872–2888. https://doi.org/10.1002/jgrd.50302.

Morales Rodriguez, C.A., 2019. Thunderstorm efficiency regimes in South America as observed by STARNET and TRMM. J. Geophys. Res.-Atmos. 124, 11428–11451. https://doi.org/10.1029/2019JD030950.

Morgan, G., 1992. THETAPLOT, an equivalent potential temperature diagram. Meteorl. Atmos. Phys. 47, 259–265. https://doi.org/10.1007/BF01025622.

Pasko, V.P., Stanley, M.A., Mathews, J.D., Inan, U.S., Wood, T.G., 2002. Electrical discharge from a thundercloud top to the lower ionosphere. Nature 416 (6877), 152–154. https://doi.org/10.1038/416152a.

Ranganathan, P., Pramesh, C.S., Aggarwal, R., 2017. Common pitfalls in statistical analysis: logistic regression. Perspect. Clin. Res. 8, 148–151. https://doi.org/10.4103/picr.PICR_87_17.

Rasmussen, E.N., Straka, J.M., 1998. Variations in supercell morphology. Part I: Observations of the role of upper-level storm-relative flow. Mon. Weather Rev. 126, 2406–2421. https://doi.org/10.1175/1520-0493(1998)126<2406:VISMPI>2.0.CO;2.

Rotunno, R., Klemp, J.B., Weisman, M.L., 1988. A theory for strong, long-lived squall lines. J. Atmos. Sci. 45, 463–485.

Ruxton, G.E., 2006. The unequal variance t-test is an underused alternative to Student's t-test and the Mann-Whitney U test. Behav. Ecol. 688-690 https://doi.org/10.1093/beheco/ark016.

Soula, S., et al., 2011. Gigantic jets produced by an isolated tropical thunderstorm near Réunion Island. J. Geophys. Res. 116, D19103. https://doi.org/10.1029/2010JD015581.

Su, H.-T., et al., 2003. Gigantic jets between a thundercloud and the ionosphere. Nature 423, 974. https://doi.org/10.1038/nature01759.

van der Velde, O.A., Montanyà, J., 2016. Statistics and variability of the altitude of elves. Geophys. Res. Lett. 43 https://doi.org/10.1002/2016GL068719.

van der Velde, O.A., Lyons, W.A., Nelson, T.E., Cummer, S.A., Li, J., Bunnell, J., 2007. Analysis of the first gigantic jet recorded over continental North America. J. Geophys. Res. 112, D20104. https://doi.org/10.1029/2007JD008575.

van der Velde, O.A., et al., 2010. Multi-instrumental observations of a positive gigantic jet produced by a winter thunderstorm in Europe. J. Geophys. Res. 115, D24301. https://doi.org/10.1029/2010JD014442.

van der Velde, O., Montanya, J., Pineda, N., Soula, S., 2013. Lightning channels emerging from the top of thunderstorm clouds. Eur. Conf. Severe Storms 2013. Helsinki, Finland. https://www.essl.org/ECSS/2013/programme/presentations/189.pdf.

van der Velde, O.A., Montanyà, J., López, J.A., et al., 2019. Gigantic jet discharges evolve stepwise through the middle atmosphere. Nature Comm. 10, 4350. https://doi.org/10.1038/s41467-019-12261-y.

Wallace, J.M., Hobbs, P.V., 2006. Atmospheric Science: An Introductory Survey, 2nd edition. Academic Press, p. 504.

Weisman, M.L., Klemp, J.B., 1984. The structure and classification of numerically simulated convective storms in directionally varying wind shears. Mon. Weather Rev. 112, 2479–2498. https://doi.org/10.1175/1520-0493(1984)112<2479:TSACON>2.0.CO;2.

Williams, E.R., Mushtak, V., Rosenfeld, D., Goodman, S., Boccippio, D., 2005. Thermodynamic conditions that lead to superlative updrafts and mixed-phase microphysics. Atmos. Res. 76, 288–306.